ChemElectroChem

Research Article
doi.org/10.1002/celc.202500202

Chemistry Europe
European Chemical Societies Publishing

www.chemelectrochem.org

The Electrochemical Shono Oxidation of *N*-Formylpyrrolidine: Mechanistic Insights from the Computational Ferrocene Electrode Model and Cyclic Voltammetry

Liana Savintseva, Paul Neugebauer, Dmitry I. Sharapa, Philipp Röse, Ulrike Krewer, and Felix Studt*

Electrochemical processes are of particular interest in modern chemical technologies as they have numerous advantages over classical approaches. While computational support for investigating thermochemical reaction mechanisms is well established, there is still no consistent methodology for modeling electrochemical processes beyond the computational hydrogen electrode. This work addresses this gap through the study of the Shono-type oxidation of *N*-formylpyrrolidine. Combining density functional theory calculations, the concept of computational Fc^+/Fc electrode, Marcus–Hush approach, and Butler–Volmer model, the reaction mechanism is elucidated, including the identification of the role and position of proton-coupled electron transfer process. Additionally, simulated cyclic voltammograms are in excellent agreement with experimental studies performed in parallel.

1. Introduction

Organic synthesis often requires harsh experimental conditions, the use of specific and often toxic catalysts, and over-stoichiometric amounts of oxidizing and reducing agents. An alternative approach can be represented by electroorganic synthesis, which has a number of advantages: 1) reduction of chemical waste, since redox agents are replaced by electricity; 2) mild reaction conditions, since strong acid or alkaline conditions are avoided, as well as high temperature or pressure; 3) inherently safe, since turning off the electricity stops the reaction and thus no thermal runaway can occur.[1] Despite the recent growing interest in electrifying chemical processes,[2,3] its wide dissemination is often hindered by a lack of detailed mechanistic understanding, which would enable a knowledge-driven approach toward process design and engineering. Although quantum chemical simulations have become a standard tool for the investigation of many chemical reactions, they are quite scarce in technical electroorganic synthesis[4,5] owing to the fact that electrochemical reactions appear to be inherently more complex. Nevertheless, modeling at the atomic and microkinetic levels has been shown to provide diverse mechanistic insights into electrode processes.[6,7] The development of theoretical approaches (also in combination with experimental investigations) would greatly advance our understanding of the underlying electrochemical reaction mechanisms and thus aid the implementation of electrochemical synthesis in the laboratory and industry.

A typical example is given by Shono oxidation (**Scheme 1**), which is used for the electrochemical functionalization of protected amines.[8–11] Although originally discovered in 1975, studies of the mechanisms of Shono-type oxidations are still scarce and controversial, such that the mechanism is still not understood in detail.[12–14] The most commonly accepted reaction pathway consists of a sequence of four reaction steps, which are an initial $1e^-$ oxidation (or electron transfer, ET) to form a radical cation (Step 1 - electrochemical), its deprotonation to a radical (Step 2 - chemical), a second $1e^-$ oxidation to form an iminium ion (Step 3 - electrochemical), and a final alcohol addition and proton elimination step (Step 4 - chemical).[8,15,16] Importantly, alternative routes involving steps of proton-coupled electron transfer (PCET) have also recently been proposed,[1] based on investigations employing density functional theory (DFT) calculations of the

L. Savintseva, D. I. Sharapa, F. Studt
Institute of Catalysis Research and Technology
Karlsruhe Institute of Technology
Hermann-von-Helmholtz-Platz 1, 76344 Eggenstein-Leopoldshafen, Germany
E-mail: felix.studt@kit.edu

P. Neugebauer, P. Röse, U. Krewer
Institute for Applied Materials – Electrochemical Technologies
Karlsruhe Institute of Technology
Adenauerring 20b, 76137 Karlsruhe, Germany

F. Studt
Institute for Technical Chemistry and Polymer Chemistry
Karlsruhe Institute of Technology
Engesserstr. 18/20, 76131 Karlsruhe, Germany

[1]It is important to note that this term can mean either a concerted transfer of an electron and a proton without any particular stable intermediate, or a sequential transfer with the presence of a stable intermediate between the electron and proton transfer.[17] In this work, PCET should always be understood as a concerted transfer.

Supporting information for this article is available on the WWW under https://doi.org/10.1002/celc.202500202

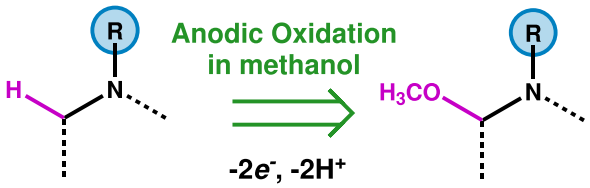

Scheme 1. Shono-type oxidation.

entire reaction sequence and experimental observations,[10] highlighting the role that theoretical simulations can play in uncovering mechanistic details in electrochemical synthesis.

The complexity of the theoretical study of electrochemical reactions lies in the need to refer to a reference electrode for which it is necessary to know its values of absolute potential. To solve this problem, we recently suggested the use of a computational ferrocene electrode (CFE) in order to investigate electrochemical reaction steps involving the transfer of electrons to or from the substrate,[18] which we think of being in close analogy to the computational hydrogen electrode (CHE) that has been used for nearly two decades[19] and highly transformative for the field of computational electro-catalysis, enabling unprecedented insights into electro-catalytic reactions such as e.g. the hydrogen evolution reaction,[20] the oxygen reduction[19] and CO_2 electroreduction[21] through simulations of PCET steps.

Herein, we employ the CFE in combination with the CHE to investigate the electrochemical oxidation of *N*-formylpyrrolidine (NFP-H) via the Shono-type reaction in methanol and in other solvents. We will show that the CFE model enables the simulation of cyclic voltammograms (CVs), thus leading to insights into its mechanistic details. Furthermore, the outcome of our theoretical simulations is compared to the experiment in order to validate the computational model and gain deeper insight into the underlying electrochemical processes.

2. Computational Methodology

DFT calculations were performed using the M06/def2-TZVP method with Grimme D3 correction and the implicit solvation model SMD[22] as implemented in the ORCA package.[23–25] This combination proved to be a good fit for geometric and energetic parameters of organic and metal-organic molecules (Figure S1, Supporting Information).[26–28] The Fc^+/Fc absolute potential in different solvents was determined using the thermodynamic cycle described in detail by Namazian et al.[29] The obtained values for acetonitrile (ACN), dichloroethane, and *N*,*N*-dimethylformamide are in good agreement with experimental and theoretical results (Table S1, Supporting Information).[29–35] In methanol, $E^0_{Fc^+/Fc,meth.} = 4.81$ V. For all calculations, the eclipsed (D_{5h}) configuration of Fc was used as the most stable, which is in agreement with other theoretical studies.[29]

The DFT calculated Gibbs free energies are used as our input parameters for the use of the CFE in combination with Marcus–Hush[36] (MH) theory for nonadiabatic electron transfer, as well as for the simulation of CVs through the Butler–Volmer model. The CFE gives reference to the $1e^-$ oxidation through the reaction $Fc^+ + e^- \rightarrow Fc^0$ (Scheme S1, Supporting Information).[18] For ACN, the experimentally determined potential of this reaction is 0.624 V relative to the standard hydrogen electrode (SHE),[32] which can be used as a conversion constant from CFE to SHE and vice versa.

Importantly, using the CFE in connection with Marcus–Hush theory gives us both the free energy difference as well as the free energy barrier for any given electron transfer process. Invoking the CHE, on the other hand, gives us the reaction free energy of the PCET step, whereas the reaction free energy barrier cannot be obtained. For a sequence of an electron transfer, followed by a proton transfer, the free energy difference of the latter step, however, can be easily calculated by using the CHE by subtracting the electron transfer step through CFE (**Scheme 2**). At the same time, the activation energy of PT can be obtained by searching for a transition state using DFT.

In order to obtain reaction free energy barriers of PCET steps, we have included the explicit solvent molecules in the calculation. In this case, the proton moves to the solvent molecule rather than being referenced to the gas phase as commonly applied in the CHE model. Utilization of this approach allows us to use the CFE as a universal reference for ET and PCET reactions (**Scheme 3**), and using the homogeneous PCET theory[17,37,38] allows us to obtain kinetic parameters. Here we apply both vibronically and electronically nonadiabatic, PCET theory (Scheme S2, Supporting Information, and the section nonadiabaticity in electron transfer theory of the Supporting Information).

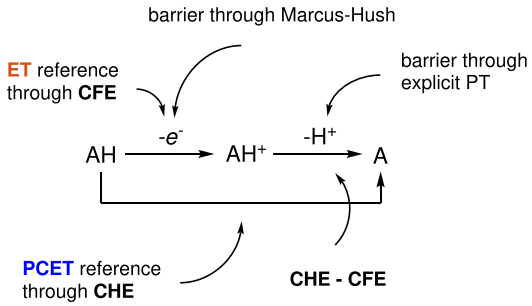

Scheme 2. Approaches for obtaining free energies (ΔG) for noncoupled electron and proton transfer steps through references to the CFE and the CHE or a combination thereof.

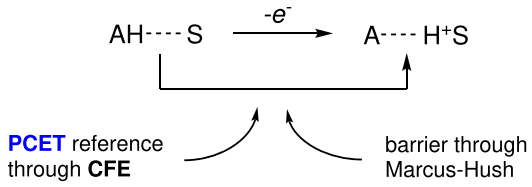

Scheme 3. Application of CFE to PCET reactions in explicit solvent media (S).

According to the Marcus–Hush theory, the reaction barriers for a $1e^-$ oxidation can be calculated as outlined in Equation (1), where $\Delta G^{\ddagger}$ is the free energy barrier, λ is the reorganization energy, F is the Faraday constant, E and E^0 are the applied and formal potentials, respectively.

$$\Delta G^{\ddagger} = \frac{\lambda}{4}\left(1 - \frac{F(E-E^0)}{\lambda}\right)^2 \tag{1}$$

The reorganization energy consists of two contributions the inner- (λ_i) and outer-sphere (λ_o) reorganization energy. λ_i is calculated through Equation (2). This equation can be understood as follows: after the fast electron transfer from the donor molecule (D) to the acceptor (A), a slow internal reorganization of the molecules from the charged states of the initial (neutral) geometries with the inner energies $U_{D^+}^{neu}$ and $U_{A^-}^{neu}$ to the equilibrium charged states with energies $U_{D^+}^{cat}$ and $U_{A^-}^{an}$.

$$\lambda_i = \left[U_{D^+}^{neu} - U_{D^+}^{cat}\right] + \left[U_{A^-}^{neu} - U_{A^-}^{an}\right] \tag{2}$$

The electron acceptor in the electrochemical oxidation is the working electrode, whose contribution to the reorganization is assumed to be zero $U_{A^-}^{neu} - U_{A^-}^{an} = 0$.[39] This four-point scheme has been extended to compute the inner-sphere reorganization energies for PCET:[17] the electron and proton are defined to be on their donors for the reactant and on their acceptors for the product (Scheme S3, Supporting Information). This can be achieved by constrained geometry optimization.

The outer-sphere reorganization energy reflects the energy expended on the reorientation and polarization of the surrounding solvent as a result of the electron transfer process (Equation (3))

$$\lambda_o = \frac{e^2}{8\pi\epsilon_0}\left(\frac{1}{a} - \frac{1}{d}\right)\left(\frac{1}{\epsilon_{op}} - \frac{1}{\epsilon_s}\right) \tag{3}$$

Here, e is the electron charge, ϵ_0 - dielectric constant of vacuum, a - molecule radii calculated from the SMD volume of the oxidized molecule, d - distance to the electrode surface, ϵ_{op} and ϵ_s - optical and static dielectric constants of the solvent ($\epsilon_{op} = n^2$, n - refractive index). For methanol, $\epsilon_{op} = 1.76$ based on $n = 1.3270$[40,41] and $\epsilon_s = 32.70$. λ_o is calculated at $d = \infty$, since we are assuming the process takes place in the bulk (Figure S2, Supporting Information).

According to Equation (1), the free energy barrier of an electrochemical process is a function of overpotential $\eta = E - E^0$. Knowing $\Delta G^{\ddagger}$, it is possible to obtain the electron transfer constant, which is obviously also a function of η. Most interesting for electrochemistry is the so-called standard electron transfer constant k_0, which is the ET constant at $\eta = 0$. In the case of the outer-sphere electron transfer, one can refer to the Arrhenius equation (Equation (4)). As a first assumption for the pre-exponential factor A, values of $A = 10^4$– 10^5 cm s^{-1} are used, which were observed in the early Marcus theory based on the collision theory.[42]

$$k_0 = A\exp\frac{-\Delta G^{\ddagger}|_{E=E^0}}{RT} \tag{4}$$

However, in practice, even for the simplest ET systems, such as iron or rhodium complexes, this factor may differ by orders of magnitude from the theoretically determined one.[42] In those cases, k_0 can be calculated directly from the MH model[43–46] (Equation (5)), where the pre-exponential factor in the nonadiabatic limit depends on the unitless reorganization energy Λ, the electrode's density of states ρ, and the electronic coupling H_{DA}^0 between the adsorbate and electrode.

$$k_0 = \frac{k_{max}}{\sqrt{4\pi\Lambda}}\exp\left[-\frac{\Lambda}{4}\right]\int_{-\infty}^{\infty}\exp\frac{\left[-\frac{\epsilon^2}{4\Lambda}\right]}{2\cosh\left[\frac{\epsilon}{2}\right]}d\epsilon \tag{5}$$

Here k_{max} is the maximal possible rate of the ET process (Equation (6)). For a more detailed explanation, see Supporting Information.

$$k_{max} = \frac{(2\pi)^2\rho H_{DA}^{0\ 2}}{\beta h} \tag{6}$$

Theoretical simulations of CVs are performed analogous to previous work.[47] Briefly, a numerical approach based on Fick's second law of linear diffusion and the Butler–Volmer formalism for the forward (k_f) and backward (k_b) reaction rates has been employed, see Equation (7) and (8).

$$k_f = k_0 e^{(1-\alpha)nF(E-E^0)/RT} \tag{7}$$

$$k_b = k_0 e^{-\alpha nF(E-E^0)/RT} \tag{8}$$

Here, α - the symmetry factor for elemental steps, and n - number of transferred electrons ($n = 1$ for a single ET step). The diffusion coefficient of the NFP-H in methanol solution was calculated using the Wilke–Chang equation[48] $D = 2.07 \cdot 10^{-5}$ cm^{2}s^{-1}. α was assumed to be 0.5, since this is a standard assumption when the symmetry factor is unknown.[49] k_0 comes from the MH model as it was described above. For the diffusion process, a simple approach called the finite-difference method based on a diffusion grid ($n \times m$, where $n = i, j, \ldots$ denotes distance to the electrode, and $m = 1, 2, \ldots, N$ denotes time steps) was used.[50] Then Fick's second law of diffusion was approximated in discrete form and then solved for the concentration of interest (Equation (9)).

$$C_{i,t} = C_{i,t-1} + \omega(C_{i-1,t-1} - 2C_{i,t-1} + C_{i+1,t-1}) \tag{9}$$

$\omega = D\Delta t/\Delta x^2$ is the simulation parameter and Δt is the time and Δx - the distance increments. $C_{i,t}$ is the concentration of a diffusing species at time t at distance i from the electrode surface. If the diffusing species are also involved in a first-order chemical reaction with the rate constant k_c^1 (the superscript indicates the reaction order), then (Equation (9)) can be rewritten as Equation (10).

$$C_{i,t} = C_{i,t-1} + \omega(C_{i-1,t-1} - 2C_{i,t-1} + C_{i+1,t-1}) - k_c^1\Delta t C_{i,t-1} \tag{10}$$

All chemical stages of the Shono-type oxidation, including pure proton transfer, are bimolecular, where a solvent molecule (methanol) is involved in the reaction. Since methanol is both the solvent and the reactant, its concentration can be taken as a constant, making it possible to move to a pseudo-first-order reaction by multiplying the rate constant by the concentration of methanol $k^1_{\text{eff}}\,[\text{s}^{-1}] = k^2_c\,[\text{l}\cdot\text{mol}^{-1}\cdot\text{s}^{-1}]\cdot C_{CH_3OH}\,[\text{mol}\cdot\text{l}^{-1}]$.

The rate of mass transfer to the electrode surface of the oxidized species (J_{Ox}) is then described in the simulator using the flux equations (Equation (11)) based on the concentrations $C_{Ox,1}$ and $C_{Red,1}$ of the oxidized and reduced forms one Δx distance increment away from the electrode surface, respectively (refer to the original source for the details[47]).

$$-J_{Ox} = \frac{k_f C_{Ox,1} - k_b C_{Red,1}}{1 + \frac{k_f \Delta x}{D} + \frac{k_b \Delta x}{D}} \tag{11}$$

And finally, the total faradaic current density that corresponds to each time increment is calculated as $i = -nFJ_{Ox}$.

3. Results and Discussion

3.1. Oxidation mechanism

The reaction mechanism of the Shono-type oxidation is given in **Scheme 4**. Obviously, there are five possible pathways: the classic four-step ECEC (1), three-step E-PCET-C (2), PCET-E-C (3), and E-C-PCET (4), and finally a two-step PCET-PCET (5).

The product of the $2e^-$ oxidation *N*-formyl-2-methoxypyrrolidine, denoted here as NFP-OMe can be further electrooxidized via an analogous Shono-type oxidation at the other α-carbon since there is still one accessible *N*-neighboring α-carbon available. The result of this oxidation is the α,α'-dimethoxy derivative, *N*-formyl-2,5-dimethoxypyrrolidine, denoted as NFP-$(OMe)_2$ (Figure S4, Supporting Information). The complete transformation chain should also include elimination products, pyrrolines (Scheme S4, Supporting Information),[16,51] the yield of which depends on the acid–base properties of the electrolyte rather than on electrochemical transformations. In this paper, we focus on the methoxy derivatives of NFP-H due to their relevance in electrochemical transformations. Furthermore, previous studies on *N*-formylpyridine in methanol/$TBABF_4$ have demonstrated that the formation of elimination products is minimal, typically ranging from 1–3%.[51]

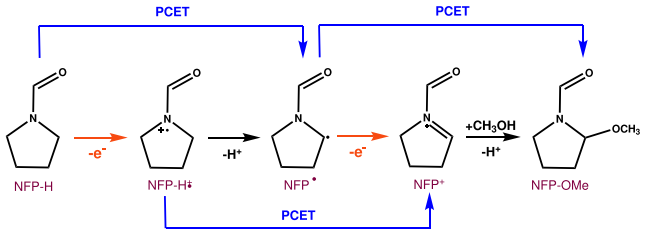

Scheme 4. Possible pathways of the NFP-H oxidation.

Utilizing the CHE as the reference, we can plot the free energy diagram of the conversion NFP-H to NFP-$(OMe)_2$ through four PCET steps (mechanism 5, Figure S5, Supporting Information). As mentioned in the introduction, this particular approach does not allow us to consider all the different mechanisms under discussion. However, according to CHE calculations, the electrode surface does not play a direct role in the oxidation process. This conclusion is supported by the fact that all neutral intermediates are physisorbed (**Table 1**, see Supporting Information), and considering the molecular size, their penetration through the electric double layer is highly improbable. This indicates the outer-sphere electron transfer is taking place and allows us to focus on the bulk calculations.

Considering the oxidation pathway further, we can exclude the possibility of the PCET conversion of NFP-H to NFP$^{\cdot}$ based on the analysis of the proton potential energy curves from the homogeneous PCET theory (Figure S7 and S8, Supporting Information): in the neutral state, the average smallest distance between the proton donor (α-carbon in NFP-H) and acceptor (oxygen in methanol molecule) is 3.34 Å (Figure S6, Supporting Information), which makes the vibronic overlap term $S_{\mu\nu} = 0$ and the proton tunneling barrier above 1 eV (Figure S7, Supporting Information). This means that the first step of Shono-type oxidation is an electron transfer, although thermodynamically, PCET is more favorable. Further analysis of the mechanism using homogeneous PCET theory is difficult due to the need to determine the characteristic time of solvent reorganization τ_s, the proton tunneling τ_P and the mutual location of the diabatic curves of the mono- and dioxidized states.

The calculated free energies of all the intermediates of the NFP-H oxidation in methanol are shown in **Figure 1**. In order to use a single reference (CFE) for all electrochemical steps, as explained above, we do not consider pure intermediates, but their complexes with methanol (so-called hybrid solvation). In this way, each intermediate is associated with two methanol molecules, as this proved to be extremely important for stabilizing the positive charge associated with the proton (see Supporting Information for details).

A PCET step in this case occurs as follows: in a dication of the type $[\text{NFP-H}\cdot 2CH_3OH]^{2+}$, the proton from the α-carbon of the NFP-H molecule transfers without barrier to the methanol dimer, where it is delocalized between two solvent molecules, forming a structure similar to a Zundel cation (**Figure 2**).

Table 1. Free energies of adsorption of NFP-H oxidation intermediates on the graphite electrode (BEEF-vdW[52,53] in VASP,[54–56] refer to Supporting Information) at a temperature of 300 K.

Intermediate	$\Delta G_{ads.}$ [eV]
NFP-H	0.22
NFP$^{\cdot}$	−0.03
NFP-OMe	0.22
NFP-OMe$^{\cdot}$	0.13
NFP-$(OMe)_2$	0.27

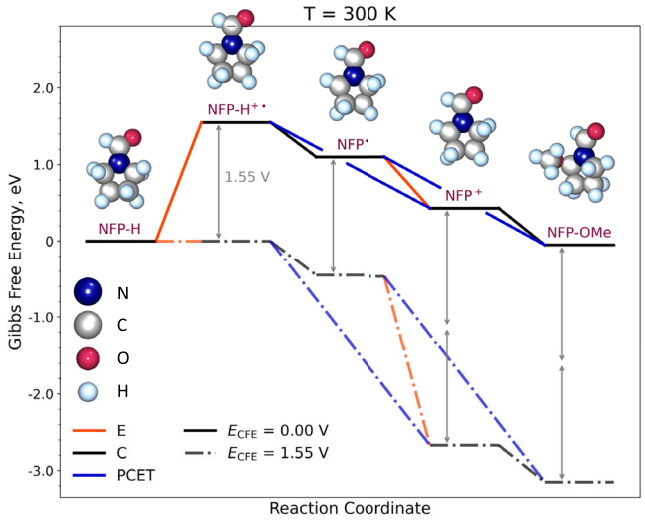

Figure 1. Free energy diagram (excluding activation barriers) of the NFP-H oxidation in bulk at 0 (solid line) and 1.55 V (dashed line) *vs.* CFE. Each intermediate is associated with two methanol molecules.

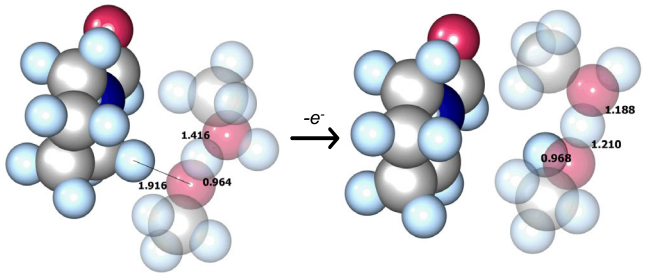

Figure 2. Illustration of PCET NFP-H$^{+\cdot}$ → NFP$^{\cdot}$ (methanol dimer is transparent).

The barriers for the electrochemical steps were calculated using Equation (1), λ_i and λ_o are given in **Table 2**. ET steps represent the classical Marcus–Hush case, where $\lambda_i < \lambda_o$ i.e., the nonadiabatic case, for which Equation (5) for k_0 can be applied. PCET steps cannot be adequately described by the Marcus–Hush theory, which assumes a nonadiabatic, single-electron transfer with relatively small inner-sphere reorganization. In our case, however, the inner-sphere reorganization energy for PCET steps dominates over the outer-sphere contribution (Table 2). As discussed above, the homogeneous PCET theory should be applied.[52–56]

Table 2. Inner-sphere (λ_i), outer-sphere (λ_o) and total (λ) reorganization energies in eV for NFP-H oxidation in methanol solution, as well as free energy barriers at 300 K ($\Delta G^{\ddagger}$, eV) at 0 (1.55) V vs. Fc$^+$/Fc and standard electron transfer constants (k_0, cm s^{-1}).

Stage	λ_i	λ_o	λ	$\Delta G^{\ddagger}$	k_0
NFP-H → NFP-H$^{+\cdot}$	0.24	0.69	0.93	1.73 (0.23)	2.8×10^{-2}
NFP-H$^{+\cdot}$ → NFP$^+$ (PCET)	1.71	0.63	2.34	0.16 (0.02)	2.0×10^{-8}
NFP → NFP$^+$	0.44	0.70	1.14	0.01 (0.43)	3.3×10^{-3}
NFP → NFP-OMe (PCET)	1.32	0.55	1.87	0.07 (0.10)	2.2×10^{-6}
NFP-OMe → NFP-OMe$^{+\cdot}$	0.29	0.65	0.94	1.91 (0.34)	2.5×10^{-2}

The free energy diagram with the barriers is given in **Figure 3**A. We consider the conversion at $E = 1.55$ V vs. Fc$^+$/Fc, a potential at which the free energy of all intermediates is below or at the same level as the initial state (the potential that is assumed to be the potential-determining within the CHE model). It becomes obvious that the most kinetically preferable path is E-PCET-C with the following barriers 0.23, 0.01, and 0.08 eV. The path E-C-PCET has comparable barriers of 0.23, 0.03, and 0.10 eV, respectively. In any case, we found that the first electron transfer is the most difficult, which is consistent with the experiment (Supporting Information).

To calculate the values of the standard ET constant, refer to Equation (5) and (6), where H^0_{DA} for the outer-sphere case is 0.6 kJ mol,[46] β - the attenuation constant in cm^{-1}, is equal to $\sim 10^8$ for saturated organic liquids,[45] and $\Lambda = \frac{\lambda}{k_B T}$. The electron density of the electrode near the Fermi level ρ was assumed to be 0.5 eV^{-1}, since this value for fcc carbon is 0.5 eV^{-1}[57] and for graphite is approximately 0.5–1.0 eV^{-1}.[58] Changes in λ have a significant impact on k_0; for example, a change in λ of just 0.1 eV can alter k_0 by a factor of 3. The obtained values of k_0 are listed in Table 2.

As discussed above, our model assumes an outer-sphere electron transfer mechanism, as no strong adsorption on the electrode surface is observed. However, future extensions of the model will also have to focus on the interaction between the molecule and the electrode surface, which in turn necessitates modeling of an explicit Helmholtz layer.

3.2. Cyclic Voltammetry Simulation

Now we turn toward simulating cyclic voltammograms using the calculated ET rate constants k_0 for each elementary step and Equation (7)–(11) and the calculated diffusion constants (D is assumed to be the same for all intermediates as for the reagent molecule NFP-H). **Figure 4** shows the voltammogram and the energy diagrams of the reaction at different applied potentials: the beginning of the first half-reaction (NFP-H oxidation), the peak potential of the first half-reaction, the beginning of the second half-reaction (NFP-OMe oxidation), and finally the peak potential of the second half-reaction. It can be seen that the oxidation peaks of the first and second oxidations are separated by 0.18 V.

A comparison with the experiment (**Figure 5**A) shows that we have correctly identified the oxidation mechanism, since the positions of the peaks match. We note that the simulated current in the presence of methanol does not match the experimental value and is, in fact, underestimated, which we attribute to complex processes of methanol oxidation near the electrode rather than inaccuracies in the diffusion coefficient estimation. In addition, our simulation model is very simple and does not include such complex components of the electrochemical interface as the electrical double layer, the surface imperfections, or the salt effect.

Interestingly, although the further oxidation of NFP-OMe makes a significant contribution to the current during the CV scanning (Figure 4A and S14, Supporting Information), this

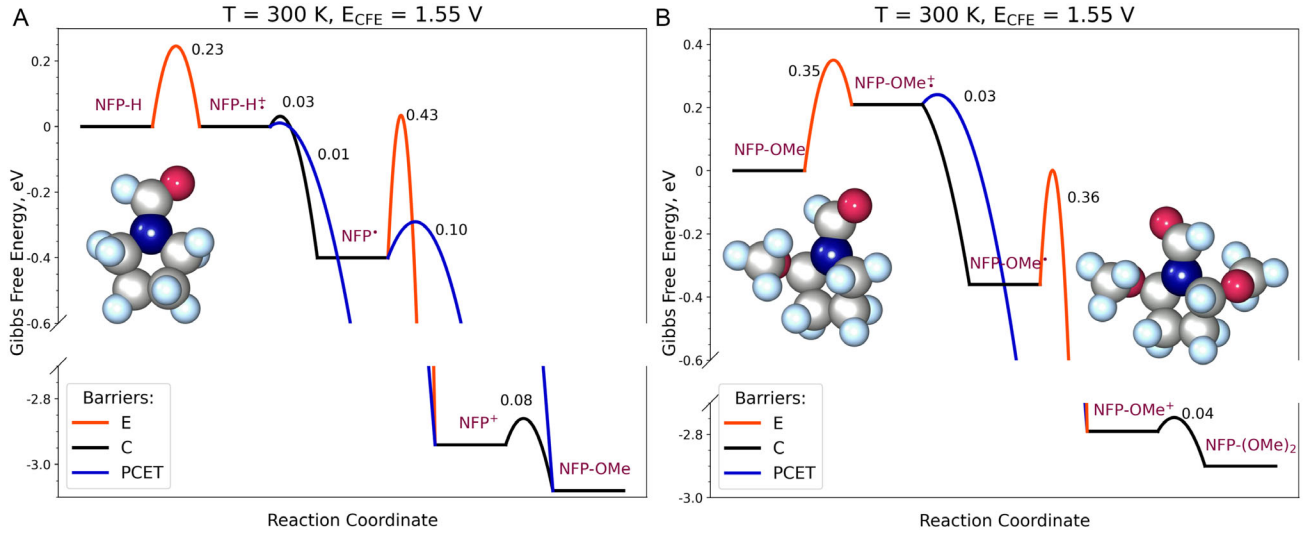

Figure 3. Energy diagram illustrating the transformation of A) NFP-H to NFP-OMe, and B) NFP-OMe to NFP-$(OMe)_2$ via the mechanisms discussed.

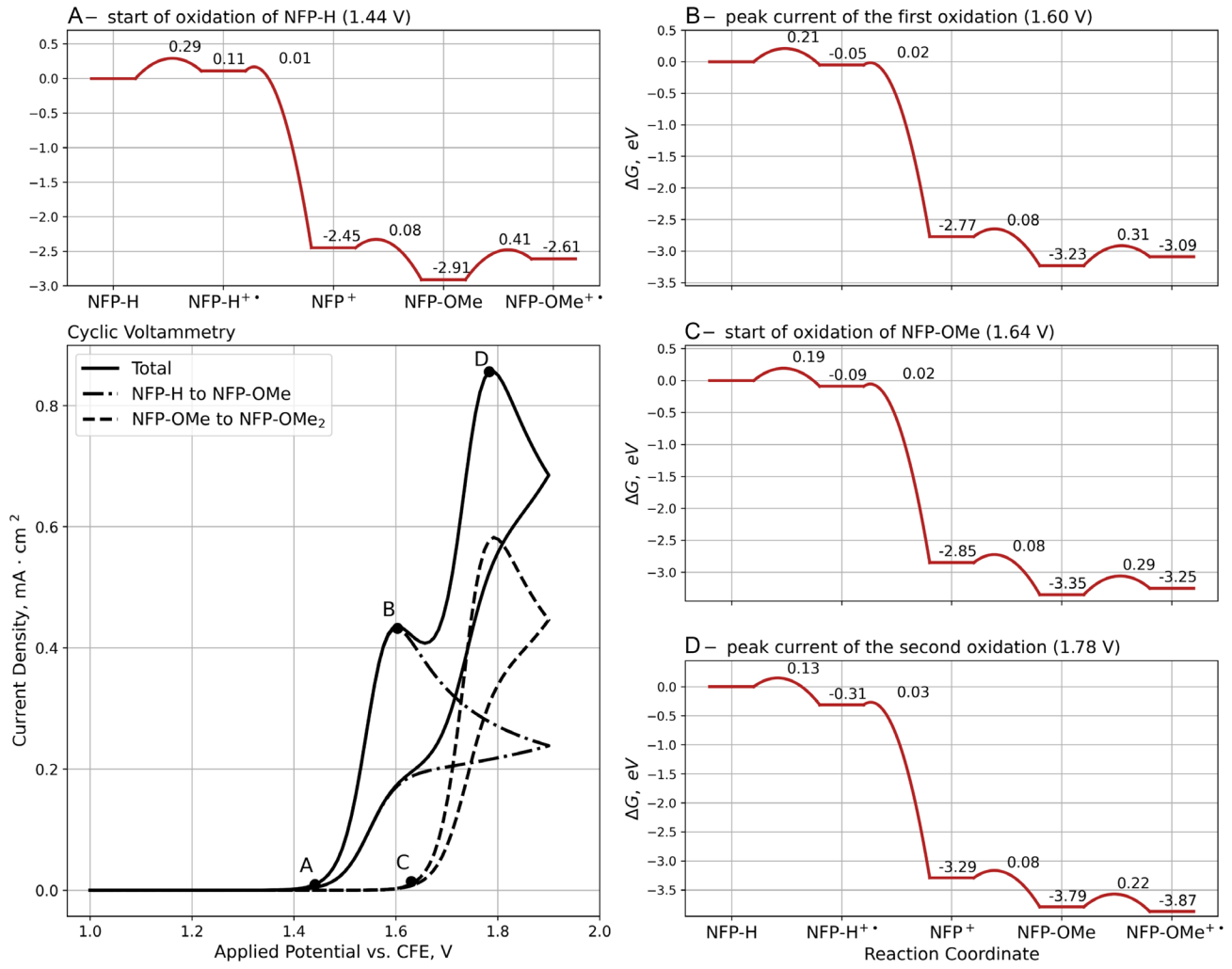

Figure 4. Simulated CV between 1 and 1.95 V ($v = 0.25\ mV{\cdot}s^{-1}$) of the NFP-H oxidation in methanol and the energetic profiles of the reaction at different applied potentials A–D) according to mechanism 2.

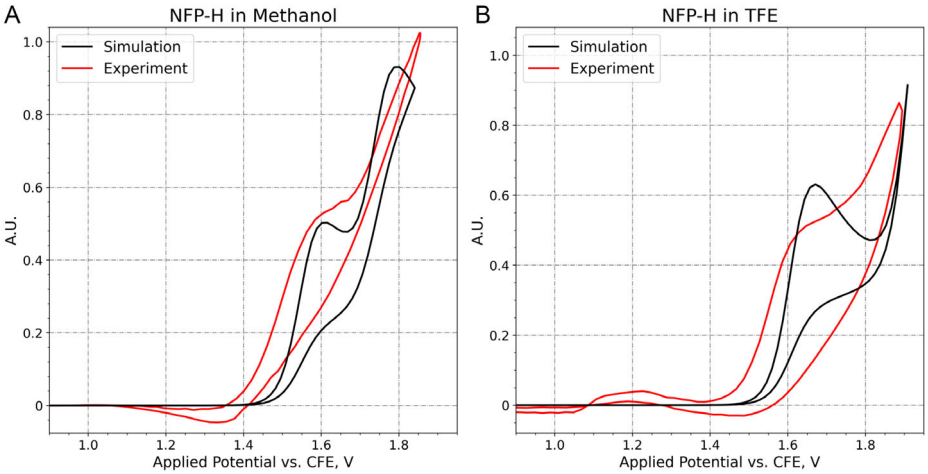

Figure 5. Simulated and experimental CVs (between 0.5 and 1.85 V vs. Fc^{+}/Fc) for NFP-H oxidation to NFP-$(OMe)_2$ A) in methanol and B) in TFE (steady state cycles were taken: 7th for the simulations and 10th and 7th for the experiment in methanol and TFE, respectively), C(NFP-H) = 5 mM, $v = 25\ mV\ s^{-1}$.

process is practically reversible and results in only a small amount of the overoxidized product NFP-$(OMe)_2$ (Figure S15, Supporting Information).

Note that the oxidation process takes place in methanol, which is easily oxidized under these conditions.[59,60] The oxidation potential of the first oxidation step of methanol (a PCET step) was determined to be 1.64 V vs. CFE (Figure S9B, Supporting Information) and all subsequent steps have lower potentials. This suggests that methanol oxidation overlaps with the oxidation peaks of NFP-H, in agreement with experimental observations (Figure S12A, Supporting Information). Although the oxidation curve of NFP-H can be obtained by subtracting the background curve, we cannot exclude the possibility that more complex processes involving methanol oxidation of intermediates occur near the electrode surface, potentially influencing the oxidation kinetics of the molecule. Furthermore, calculations using the CHE model indicate the potential electrocatalytic nature of methanol oxidation (Figure S10, Supporting Information). In this case, the model would also need to account for the adsorption and desorption of intermediates on the electrode surface. However, since this has not yet been implemented, we do not consider this process in this paper.

In order to gauge the influence of the solvent, we performed a simulation of NFP-H electrooxidation in trifluoroethanol (TFE). TFE meets the requirements for electro-induced reactions, having a relatively low viscosity (1.75 mPa·s at 25°) and being electrochemically stable in a wide range of potentials.[60] To confirm the stability of TFE, its oxidation potentials were calculated. The bulk oxidation mechanism was found to be similar to that of methanol, i.e., each step represents a concerted PCET transfer. The potential of TFE oxidation is 2.23 V (Figure S11, Supporting Information), which is much higher than the corresponding values for methanol (1.64 V). Thus, it is obvious that TFE does not oxidize at the operating potential required to oxidize NFP-H. The resulting CV is presented in Figure 5B, clearly illustrating the identification of the oxidation peaks. Since the solvent is electrochemically inert under these conditions, we can be confident that only the substrate is contributing to the CV.

4. Conclusions

In summary, this study uses a combination of the CFE with Marcus–Hush theory to investigate the Shono-type oxidation of *N*-formylpyrrolidine in methanol and TFE. While the CFE model has so far been shown to be able to model the kinetics and thermodynamics of electron transfer steps, we show here how proton transfer and PCET steps can be included in this computational model. By doing so, we have been able to obtain the kinetics of all steps of the Shono-type oxidation, for both the first and second methoxylation steps. Importantly, our methodology allows us to calculate the kinetic barriers of all steps as a function of the electrochemical potential and thus enables us to simulate CVs with additional input of diffusion constants, also estimated from theoretical considerations. Our simulated CVs match those from our experimental efforts quite well, highlighting the high applicability of the CFE. Our simulations reveal that the Shono oxidation of NFP is occurring via the E-PCET-C mechanism for both methoxylation steps. We furthermore identified that the use of methanol complicates the investigation of the reaction kinetics, as the oxidation of methanol occurs at a very similar potential as the second Shono oxidation step, as also confirmed by experiments. The use of TFE alleviates this, allowing NFP-H to be oxidized without oxidizing the solvent. This study hence highlights that our method can be very useful to obtain kinetic data as a function of applied potential to the extent that the mechanistic details of underlying reaction mechanisms can be revealed.

Extensions of the current model may include tackling factors such as electrolyte salts, the electrode surface, and a better description of the Helmholtz layer to more rigorously reflect the complexity of the actual electrochemical interface. We note, however, that even though our model is quite simplistic, it provides a practical workflow for rapid mechanistic, thermodynamic,

and kinetic analyses of electrochemical oxidation or reduction reactions, as exemplified here for the Shono-type oxidation.

Future work will aim at extending our model to include effects from the Helmholtz layer, e.g., by including screening from electrolytes present at this interface.

5. Experimental Section

Materials and chemicals sections can be found in the Supporting Information. An undivided glass cell was filled with methanol/$TBABF_4$ or Trifluorethanol/$TBABF_4$ (0.2 mol·L^{-1}, 100 mL). The electrolyte was purged with argon before each experiment, and a 0.2 L·min^{-1} Ar flow was purged constantly above the electrolyte during the measurements. Glassy carbon (A = 0.1963 cm^2) was assembled as the working electrode, a Pt-sheet (2 cm^2) as counter electrode, and an Ag/AgCl (KCl_{sat} in H_2O) as the reference electrode. The constant conversion potential from Ag/AgCl to Fc^+/Fc is −0.49 V (c.f. Figure S3, Supporting Information). Potentials were *iR* corrected by the bulk resistance R_u determined by potentiostatic electrochemical impedance spectroscopy at OCP before each experiment in the high frequency region from 1 MHz to 100 kHz at a phase angle of $\phi = 0°$; the amplitude was set to $\Delta E_{AC} = 10\ mV_{rms}$. All measurements were conducted at 25 °C and 1 bar. CV measurements of the electrolyte were conducted in the potential range from 1.0 to 2.4 V vs. Ag/AgCl with scan rates of 200, 100, 50, and 25 mV·s^{-1} for 30, 30, 20, and 10 cycles, respectively. After the sequence was finished, NFP-H (48.6 μL, 5 mmol·L^{-1}) was added, and it was stirred vigorously for 1 min. Then the sequence was repeated. At the end of each experiment, a small amount of ferrocene was added and cyclic voltammograms were conducted for 5 cycles at 100 mV·s^{-1} in a potential range from 0 to 1.0 V vs. Ag/AgCl.

Acknowledgements

The authors acknowledge the financial support by the BMFTR Federal Ministry of Research, Technology and Space of Germany as part of the Cluster4Future ETOS (Electrifying Technical Organic Electrosynthesis) and the project Digital Electrolyzer Design for Technical Organic Synthesis (DigiE-tos, 03ZU1205NA and 03ZU1205NB). Also, the authors thank for support by the state of Baden–Württemberg through bwHPC and by the DFG through grant no. INST 40/575-1 FUGG (JUSTUS 2 cluster, RVs bw17D011). Financial support from the Helmholtz Association is also gratefully acknowledged.

Conflict of Interest

The authors declare no conflict of interest.

Data Availability Statement

The data that support the findings of this study are openly available in [KITopen] at [https://doi.org/10.35097/yb7ufn2442ndv3vj], reference number [1000182376]. A python script for CV simulation is also available at [https://doi.org/10.35097/q0sh3rj5qw3tcsag], reference number [1000181943], and as a project on GitHub.

Keywords: computational ferrocene electrode · cyclic voltammetry · density functional theory · Marcus–Hush theory · Shono oxidation

[1] A. Wiebe, T. Gieshoff, S. Möhle, E. Rodrigo, M. Zirbes, S. R. Waldvogel, *Angew. Chem. Int. Ed.* **2018**, *57*, 5594.
[2] C. Zhu, N. W. J. Ang, T. H. Meyer, Y. Qiu, L. Ackermann, *ACS Cent. Sci.* **2021**, *7*, 415.
[3] C. Schotten, T. P. Nicholls, R. A. Bourne, N. Kapur, B. N. Nguyen, C. E. Willans, *Green Chem.* **2020**, *22*, 3358.
[4] T. Ali, H. Wang, W. Iqbal, T. Bashir, R. Shah, Y. Hu, *Adv. Sci.* **2022**, *10*.
[5] P. Röse, P. Neugebauer, S. Tamang, S. R. Waldvogel, U. Krewer, *Chem. Ing. Tech.* **2025**.
[6] G. D. Wehinger, M. Ambrosetti, R. Cheula, Z.-B. Ding, M. Isoz, B. Kreitz, K. Kuhlmann, M. Kutscherauer, K. Niyogi, J. Poissonnier, R. Réocreux, D. Rudolf, J. Wagner, R. Zimmermann, M. Bracconi, H. Freund, U. Krewer, M. Maestri, *Chem. Eng. Res. Des.* **2022**, *184*, 39.
[7] B. J. Etzold, U. Krewer, S. Thiele, A. Dreizler, E. Klemm, T. Turek, *Chem. Eng. J.* **2021**, *424*, 130501.
[8] T. Shono, H. Hamaguchi, Y. Matsumura, *J. Am. Chem. Soc.* **1975**, *97*, 4264.
[9] T. Shono, Y. Matsumura, K. Tsubata, *J. Am. Chem. Soc.* **1981**, *103*, 1172.
[10] L. F. T. Novaes, J. S. K. Ho, K. Mao, K. Liu, M. Tanwar, M. Neurock, E. Villemure, J. A. Terrett, S. Lin, *J. Am. Chem. Soc.* **2022**, *144*, 1187.
[11] A. A. Folgueiras-Amador, K. E. Jolley, P. R. Birkin, R. C. Brown, D. Pletcher, S. Pickering, M. Sharabi, O. de Frutos, C. Mateos, J. A. Rincón, *Electrochem. Commun.* **2019**, *100*, 6.
[12] S. Suga, M. Okajima, J.-i. Yoshida, *Tetrahedron Lett.* **2001**, *42*, 2173.
[13] T. Hardwick, R. Cicala, T. Wirth, N. Ahmed, *Sci. Rep.* **2020**, *10*.
[14] A. M. Jones, C. E. Banks, *Beilstein J. Org. Chem.* **2014**, *10*, 3056.
[15] F. Wang, M. Rafiee, S. S. Stahl, *Angew. Chem. Int. Ed.* **2018**, *57*, 6686.
[16] T. Golub, J. Y. Becker, *Electrochim. Acta* **2016**, *205*, 207.
[17] R. E. Warburton, A. V. Soudackov, S. Hammes-Schiffer, *Chem. Rev.* **2022**, *122*, 10599.
[18] A. S. Kramarenko, D. I. Sharapa, E. A. Pidko, F. Studt, *J. Phys. Chem. A* **2024**, *128*, 9063.
[19] J. K. Nørskov, J. Rossmeisl, A. Logadottir, L. Lindqvist, J. R. Kitchin, T. Bligaard, H. Jónsson, *J. Phys. Chem. A* **2004**, *108*, 17886.
[20] J. Greeley, T. F. Jaramillo, J. Bonde, I. Chorkendorff, J. K. Nørskov, *Nat. Mater.* **2006**, *5*, 909.
[21] A. A. Peterson, F. Abild-Pedersen, F. Studt, J. Rossmeisl, J. K. Nørskov, *Energy Environ. Sci.* **2010**, *3*, 1311.
[22] A. V. Marenich, C. J. Cramer, D. G. Truhlar, *J. Phys. Chem. B* **2009**, *113*, 6378.
[23] F. Neese, *WIREs Comput. Mol. Sci.* **2011**, *2*, 73.
[24] F. Neese, F. Wennmohs, U. Becker, C. Riplinger, *J. Chem. Phys.* **2020**, *152*.
[25] F. Neese, *WIREs Comput. Mol. Sci.* **2022**, *12*.
[26] R. Valero, R. Costa, I. de P. R. Moreira, D. G. Truhlar, F. Illas, *J. Chem. Phys.* **2008**, 128.
[27] M. Isegawa, F. Neese, D. A. Pantazis, *J. Chem. Theory Comput.* **2016**, *12*, 2272.
[28] J. L. Borioni, M. Puiatti, D. M. A. Vera, A. B. Pierini, *Phys. Chem. Chem. Phys.* **2017**, *19*, 9189.
[29] M. Namazian, C. Y. Lin, M. L. Coote, *J. Chem. Theory Comput.* **2010**, *6*, 2721.
[30] M. Z. Makoś, P. K. Gurunathan, S. Raugei, K. Kowalski, V.-A. Glezakou, R. Rousseau, *J. Phys. Chem. Lett.* **2022**, *13*, 10005.
[31] M. Namazian, M. L. Coote, *J. Phys. Chem. A* **2007**, *111*, 7227.
[32] V. V. Pavlishchuk, A. W. Addison, *Inorg. Chim. Acta* **2000**, *298*, 97.
[33] D. J. Fermin, R. Lahtinen, *Dynamic Aspects of Heterogeneous Electron-Transfer Reactions at liquid|Liuid Interfaces*, pp. 179–227, Surfactant Science Series. 95, Marcel Dekker Inc., New York **2001**, ed. by Alexander G. Volkov.
[34] D. Bao, B. Millare, W. Xia, B. G. Steyer, A. A. Gerasimenko, A. Ferreira, A. Contreras, V. I. Vullev, *J. Phys. Chem. A* **2009**, *113*, 1259.
[35] A. A. Isse, A. Gennaro, *J. Phys. Chem. B* **2010**, *114*, 7894.
[36] R. A. Marcus, *Rev. Modern Phys.* **1993**, *65*, 599.
[37] J. H. Skone, A. V. Soudackov, S. Hammes-Schiffer, *J. Am. Chem. Soc.* **2006**, *128*, 16655.
[38] Y.-C. Lam, A. V. Soudackov, S. Hammes-Schiffer, *J. Phys. Chem. C* **2020**, *124*, 27309.

[39] Y. Zeng, R. B. Smith, P. Bai, M. Z. Bazant, *J. Electroanal. Chem.* **2014**, *735*, 77.
[40] M. N. Polyanskiy, *Sci. Data* **2024**, *11*.
[41] K. Moutzouris, M. Papamichael, S. C. Betsis, I. Stavrakas, G. Hloupis, D. Triantis, *Appl. Phys. B* **2013**, *116*, 617.
[42] Z. He, Y. Chen, E. Santos, W. Schmickler, *Angew. Chem. Int. Ed.* **2018**, *57*, 7948.
[43] C. E. D. Chidsey, *Science* **1991**, *251*, 919.
[44] S. W. Feldberg, *Anal. Chem.* **2010**, *82*, 5176.
[45] P. P. Edwards, H. B. Gray, M. T. J. Lodge, R. J. P. Williams, *Angew. Chem. Int. Ed.* **2008**, *47*, 6758.
[46] M. J. Honeychurch, *Langmuir* **1999**, *15*, 5158.
[47] J. H. Brown, *J. Chem. Educ.* **2015**, *92*, 1490.
[48] C. R. Wilke, P. Chang, *AIChE J.* **1955**, *1*, 264.
[49] A. M. Román, J. Dudoff, A. Baz, A. Holewinski, *ACS Catal.* **2017**, *7*, 8641.
[50] D. Britz, *Digital Simulation in Electrochemistry: Third Completely Revised and Extended Edition with Supplementary Electronic Material*, Springer Berlin Heidelberg **2005**.
[51] T. Golub, J. Y. Becker, *Electrochim. Acta* **2015**, *173*, 408.
[52] J. Klimeš, D. R. Bowler, A. Michaelides, *J. Phys.: Condens. Matter* **2009**, *22*, 022201.
[53] J. Klimeš, D. R. Bowler, A. Michaelides, *Phys. Rev. B* **2011**, *83*.
[54] G. Kresse, J. Hafner, *Phys. Rev. B* **1993**, *47*, 558.
[55] G. Kresse, J. Furthmüller, *Comput. Mater. Sci.* **1996**, *6*, 15.
[56] G. Kresse, J. Furthmüller, *Phys. Rev. B* **1996**, *54*, 11169.
[57] A. Tapia, G. Canto, G. Murrieta, R. de Coss, *J. Exper. Theor. Phys. Lett.* **2005**, *82*, 120.
[58] M. Klintenberg, S. Lebègue, C. Ortiz, B. Sanyal, J. Fransson, O. Eriksson, *J. Phys.: Condens.Matter* **2009**, *21*, 335502.
[59] D. Y. Chung, K.-J. Lee, Y.-E. Sung, *J. Phys. Chem. C* **2016**, *120*, 9028.
[60] K. Shirai, T. Hamamoto, T. Maki, O. Onomura, N. Kise, Y. Aoyama, Y. Matsumara, *J. Electroanal. Chem.* **2001**, *507*, 191.

Manuscript received: May 22, 2025
Revised manuscript received: June 16, 2025
Version of record online: